

# Spontaneous Lateral Composition Modulation in AlAs/InAs Short Period Superlattices Via the Growth Front

J. MIRECKI MILLUNCHICK, R.D. TWESTEN, S.R. LEE,  
D.M. FOLLSTAEDT, and E.D. JONES

Sandia National Laboratory, Albuquerque, NM

S.P. AHRENKIEL, Y. ZHANG, H.M. CHEONG, and A. MASCARENHAS

National Renewable Energy Laboratory, Golden, CO

The spontaneous formation of lateral composition modulation in AlAs/InAs short period superlattices on InP (001) substrates has been investigated. Transmission electron microscopy and x-ray diffraction reciprocal space mapping show that the lateral modulation is very regular, with a periodicity along the [110] direction on the order of 180 Å. A surprising result is that this material system also exhibits a lateral modulation along the  $[\bar{1}\bar{1}0]$  direction, with a periodicity of 330 Å. Reflection high energy electron diffraction performed during the deposition revealed that the reconstruction changed from  $(2 \times 1)$  during the InAs deposition cycle to  $(1 \times 2)$  during the AlAs cycle, which may be related to the presence of the modulation in both  $\langle 110 \rangle$  directions. High magnification transmission electron micrographs show that the surface is undulated and that these undulations correlate spatially with composition modulation. Detailed analysis of the images shows that the contrast observed is indeed due to composition modulation. Photoluminescence from the modulated layer is strongly polarized and red-shifted by 220 meV.

**Key words:** Composition modulation, lateral modulation, superlattices

## INTRODUCTION

The role of surface morphology in the growth of heteroepitaxial films is a key issue in the realm of strain relaxation.<sup>1</sup> It is now well accepted that a rough morphology can relieve strain without the introduction of misfit dislocations. Experimentally, this has been observed as coherent arrays of ripples or faceted islands that partially relieve the strain.<sup>1</sup> Relaxation occurs because the lattice can relax the strain at the crest of the ripple, producing an overall reduction in strain in spite of the complementary compression of the lattice planes at the troughs. This type of phenomenon has been treated theoretically by morphological instability continuum models,<sup>2-4</sup> and by more atomistic approaches.<sup>5-7</sup>

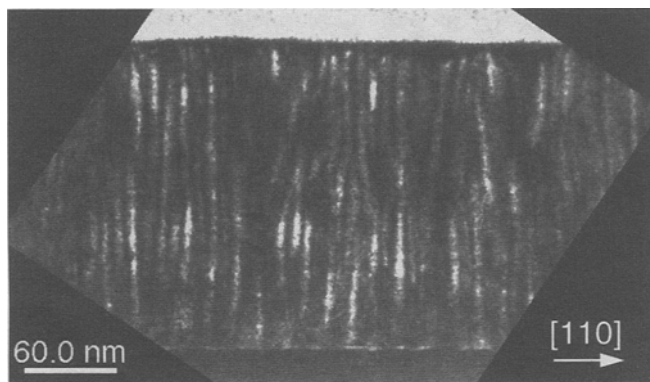
Recently, lateral composition modulation has been shown to be correlated with the surface morphology of the film,<sup>8</sup> as predicted by morphological instability models for alloy thin films.<sup>9</sup> Lateral modulation has

been observed for a wide range of compound semiconductors during homogeneous growth<sup>10</sup> and short period superlattice growth,<sup>8,11-14</sup> which is an interesting case to study because it yields particularly strong and regular spontaneous lateral modulation. This article describes spontaneous lateral composition modulation as a result of the deposition of AlAs<sub>m</sub>/InAs<sub>n</sub> short period superlattices on InP (001) substrates, where *m* and *n* are the number of monolayers (ML) deposited for each binary compound ( $n \approx m \approx 2$  ML).

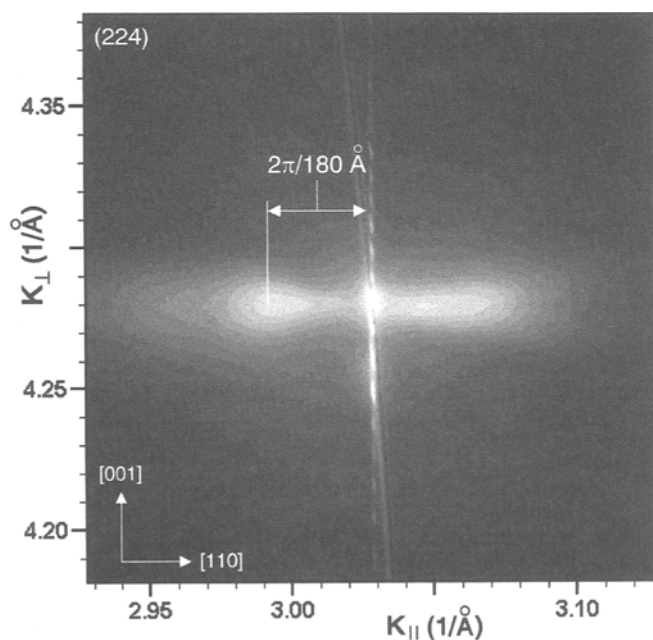
## EXPERIMENTAL

All short period superlattice (SPS) structures were deposited on semi-insulating InP (001) wafers using molecular beam epitaxy. The InP surface was prepared by heating the surface under an As overpressure. Typical structures consist of a nominally lattice-matched InAlAs buffer layer, followed by a AlAs<sub>m</sub>/InAs<sub>n</sub> SPS with various values of *m* and *n*. The effect of altering *m* and *n* was to change the average In composition, thus the average strain *f*, of the SPS layer. For this study, *f* was varied from *f* = 0% (lattice

(Received March 3, 1997; accepted April 24, 1997)



a



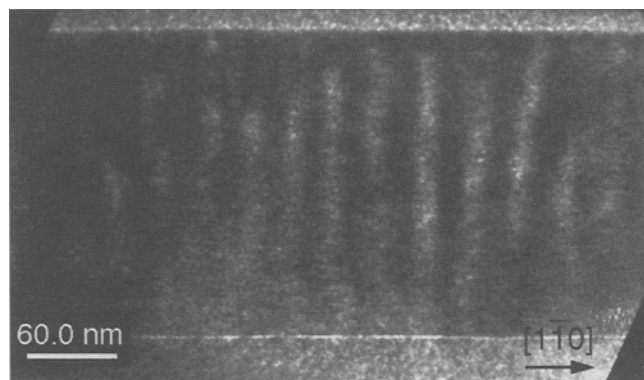
b

Fig. 1. (a) Cross-sectional TEM with  $g = 002$  in the  $[1\bar{1}0]$  projection of an  $\text{AlAs}_{1.46}/\text{InAs}_{1.55}$  SPS that is compositionally modulated. (b) X-ray reciprocal space map of the structure projected onto the  $[1\bar{1}0]$  plane. The lobes to either side of the Bragg peak reflect the lateral periodicity of  $\lambda \sim 180\text{\AA}$  of the composition modulation. The TEM contrast variation has a shorter apparent modulation wavelength due to the oscillatory nature of the contrast, as described in the text.

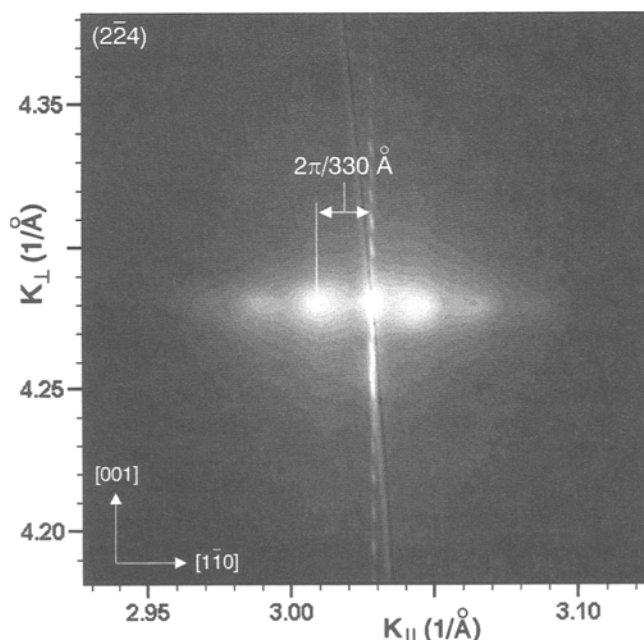
matched) to  $f = -0.6\%$  (tensile strain). The other growth conditions were kept nominally constant, with a growth temperature of  $530^\circ\text{C}$  and total alloy growth rate on the order of  $0.7\text{ ML/s}$  as calibrated by reflection high energy electron diffraction (RHEED). The films were characterized using transmission electron microscopy (TEM), x-ray diffraction reciprocal space mapping, and polarized photoluminescence (PPL). TEM samples were prepared either in cross-section, using mechanical polishing followed by Ar-ion milling, or in plan-view, by back-thinning with a selective chemical etch to remove the substrate followed by Ar-ion milling. Images were obtained using either 200 or 300 keV electrons under various imaging conditions.

#### MICROSTRUCTURAL CHARACTERIZATION

Figure 1a shows a dark-field cross-sectional TEM



a



b

Fig. 2. (a) Cross-sectional transmission electron micrograph with  $g = 002$  in the  $[110]$  projection of the  $\text{AlAs}_{1.44}/\text{InAs}_{1.56}$  SPS that is compositionally modulated. (b) X-ray reciprocal space map of the structure projected onto the  $[110]$  plane. The lobes to either side of the Bragg peak reflect the lateral periodicity of  $\lambda \sim 330\text{\AA}$ , in agreement with the XTEM micrograph.

micrograph in the  $[1\bar{1}0]$  projection with  $g = 002$  of an  $\text{AlAs}_{1.44}/\text{InAs}_{1.56}$  SPS that exhibits composition modulation. The very strong and regular contrast variation across the film corresponds to the modulation in composition along the  $[110]$  direction. Figure 1b shows the x-ray reciprocal space map around the  $(224)$  reflection with the sample aligned such that the  $[1\bar{1}0]$  direction is perpendicular to the diffraction plane, as recorded using  $\text{Cu-K}\alpha$  x-rays and a position-sensitive detector.<sup>15</sup> Distinct lateral satellites are visible on either side of the primary  $(224)$  diffraction spot, corresponding to a lateral periodicity of  $180\text{\AA}$ . In addition, the satellites originating in the SPS layer line up with the  $\text{InP}$   $(224)$  substrate peak, showing that the SPS structure is lattice matched. Figure 2 shows the cross-sectional TEM and x-ray reciprocal space map of this  $\text{InAs}/\text{AlAs}$  structure in the orthogonal  $[110]$  crystallographic direction. Composition modulation is also

apparent in this image, however, it is along the  $[1\bar{1}0]$  direction and has a periodicity of  $330\text{\AA}$ . The magnitude of the modulation wavelength in both  $\langle 110 \rangle$  directions was found to be independent of the average strain across the SPS structure. To the best of our knowledge, no other material system has been reported to exhibit composition modulation in SPSs for both  $\langle 110 \rangle$  directions.

Anisotropic lateral composition modulation may be directly related to the anisotropy of the zinc-blende surface. It is well known that for GaAs (001) under group-V rich conditions, for example, the surface reconstruction is  $(2 \times 4)$ . The atomic arrangement of the surface consists of As-dimer and missing-As-dimer rows aligned along the  $[1\bar{1}0]$  direction.<sup>16</sup> Theoretical calculations of this GaAs (001) surface, show that surface diffusion is dominant along the  $[1\bar{1}0]$  direction.<sup>17</sup> RHEED patterns observed during the growth of most III-V alloys also show similar reconstruction; therefore, adatom diffusion is expected to be highly anisotropic in these samples as well.

In order to examine this phenomenon more closely, the RHEED patterns were observed during the deposition of the SPS structure. Figure 3 shows the intensity of the RHEED specular reflection during growth. The oscillations in the intensity do not correspond to the deposition of an integer monolayer; rather, each period corresponds to one cycle of the SPS deposition, as denoted by the arrows. The RHEED pattern itself changes reconstruction depending on the compound being deposited. During the InAs deposition the pattern is  $(2 \times 1)$ , and during the AlAs the pattern is  $(1 \times 2)$ . This behavior of the reconstruction was always observed, regardless of the average strain across the SPS structure. Not a great deal is known about the  $(2 \times 1)$  reconstruction, but it is thought to be a more disordered As-stabilized surface than the  $(2 \times 4)$  reconstruction.<sup>18</sup> The specular intensity changes, therefore, are associated with the transitions between the two reconstructions. Conventional RHEED oscillations corresponding to the growth rate of the film are observed as well, however, they are partially obscured by the intensity variation due to the transition between reconstructions. The RHEED patterns observed during the deposition of a InGaAs SPS do not show this type of symmetry axis reversal between the InAs and GaAs cycles of deposition, and the resulting structures do not exhibit strong modulation in both  $\langle 110 \rangle$  directions. Therefore, the change in the axis of symmetry of the reconstruction between the deposition of the InAs and AlAs may account for the presence of composition modulation in both  $\langle 110 \rangle$  directions in AlAs/InAs SPSs.

Higher magnification TEM micrographs illustrate how the morphology of the growth front affects the composition modulation in the SPS. Figure 4 shows a bright-field TEM image of a  $\text{AlAs}_{1.9}/\text{InAs}_{1.6}$  SPS film with  $g = 002$  in the  $[1\bar{1}0]$  projection. Note that this SPS structure is not lattice matched, but is in tension with an average indium concentration of 46% as measured by x-ray diffraction. In addition to lateral

contrast variation arising from composition modulation, the image distinctly shows the individual SPS layers. The SPS Fig. 4. does not appear as flat lines parallel to the surface, rather it shows strong cusps with an amplitude on the order of a few monolayers at the dark bands. The profile of these superlattice layers is indicative of a non-planar growth front which can relieve strain in the structure. For a strained film with a corrugated surface, the crest of the undulation is not constrained laterally, allowing the lattice to relax. In the case of a tensile film, this would lead to enhanced incorporation of the smaller lattice parameter alloy (Al-rich) on the tops of the undulation,

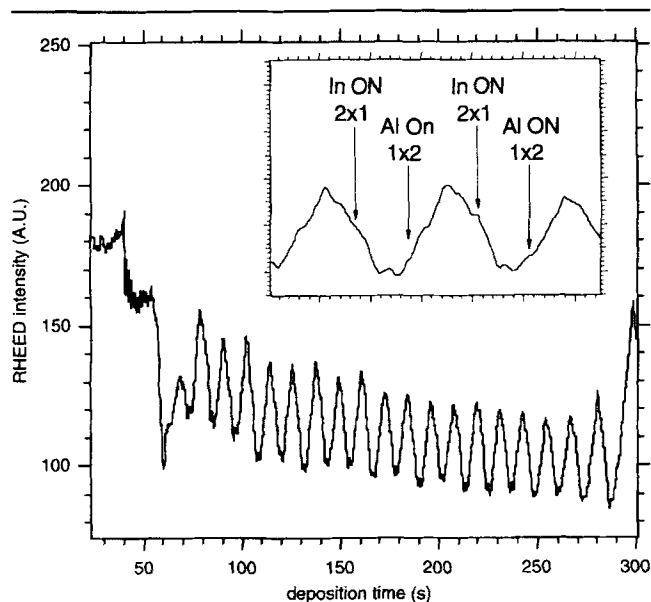


Fig. 3. RHEED intensity as a function of deposition time. The inset shows the change in RHEED intensity due to the changing surface reconstructions for InAs and AlAs deposition (indicated by the arrows).

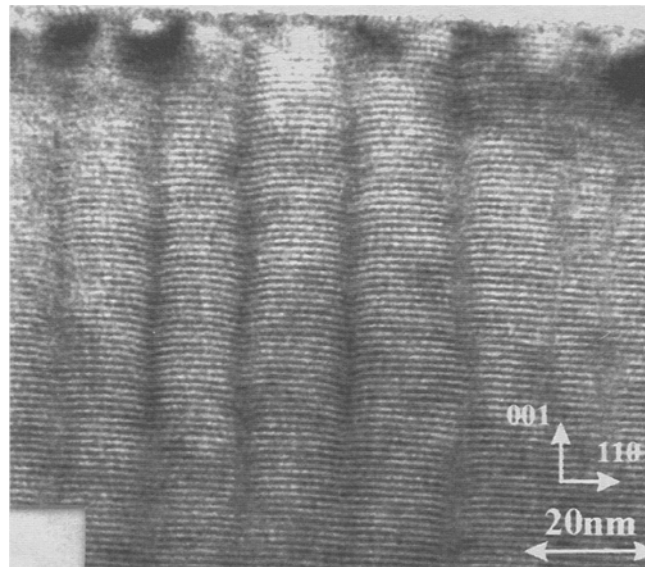


Fig. 4. Bright-field TEM image in the  $[1\bar{1}0]$  projection of the  $\text{AlAs}_{1.9}/\text{InAs}_{1.6}$  SPS in tension that is compositionally modulated. The dark-vertical bands are In-rich regions that are aligned with the troughs of the undulation.

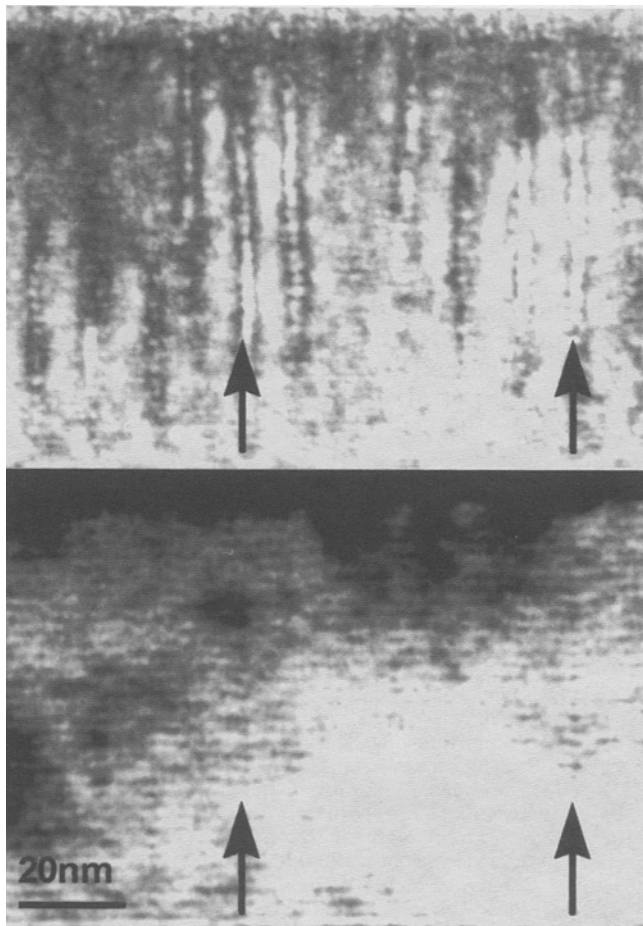


Fig. 5.  $g = (002)$  {a} and  $(004)$  {b} dark-field images of the same region of the  $\text{AlAs}_{1.9}/\text{InAs}_{1.6}$  sample. Note the lack of contrast in the  $(004)$  image, indicating the contrast for  $g = 002$  is dominated by structure factor variations. Equivalent position are marked by black arrows.

while the larger lattice parameter alloy (In-rich) would form in the troughs.<sup>9</sup> This surface undulation-composition modulation relationship was observed in all structures studied where composition modulation occurred. The undulation was extremely difficult to observe in the orthogonal  $[110]$  projection because the undulation amplitude is small compared to the modulation wavelength.

By examining dark-field images with  $g = 002$  in the two-beam mode, the troughs were identified as In-rich. In this mode, the contrast can be simply interpreted in terms of changes in the local structure factor.<sup>19</sup> The resulting image (Fig. 5a) shows strong black-white-black contrast in the regions of the SPS cusps. This behavior is a result of an oscillation in the contrast as a function of composition. For an average In composition  $x = 0.46$ , increasing  $x$  will result in decreasing image contrast until the local composition reaches  $x = 0.52$ . At this point, the average group-III scattering factor exactly equals the group-V scattering factor, causing the  $(002)$  structure factor to be kinematically forbidden and the contrast to be zero. A further increase in  $x$  causes increasing image contrast. The resulting image, therefore, is expected to consist of bright bands surrounded by narrow dark

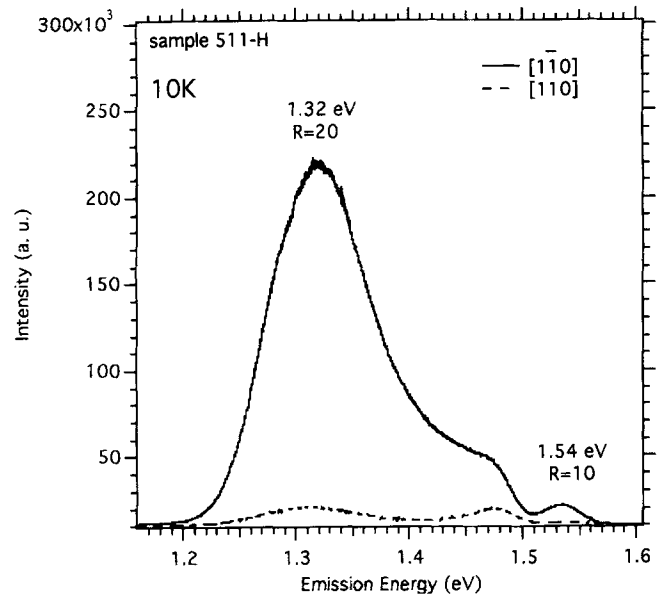


Fig. 6. Low-temperature PL spectrum taken at 10K of the  $\text{AlAs}_{1.9}/\text{InAs}_{1.6}$  SPS showing the relative intensities of the two orthogonal polarizations.

bands as the composition varies locally, in agreement with Fig. 5a. As a result of this phenomenon, the contrast variation in Fig. 1a has a smaller wavelength than the actual composition modulation. TEM image simulations for a linearly changing composition profile have shown that the peak-to-peak group-III modulation is at least 6% based on this zero in the  $(002)$  structure factor.<sup>20</sup>

That the structure factor dominates the contrast variation in these images is demonstrated by switching from an  $(002)$  to an  $(004)$  two-beam type image. Unlike the  $(002)$  reflection, contrast for the  $(004)$  reflection does not depend on the structure factor. If strain was the primary source of the image contrast, the  $(004)$  and  $(002)$  images would exhibit similar lateral contrast variation. However, the  $004$  image in Fig. 5 is uniform, indicating the lateral contrast variation in the  $(002)$  image is indeed due to composition modulation.

## OPTICAL PROPERTIES

The symmetry of the cubic lattice is broken in samples showing composition modulation. Because the binary constituent alloys are lattice mismatched, the resulting modulation of the film's crystal lattice has a component related to the lateral composition oscillation, and another associated to the strain oscillation. The strain and composition modulations are parallel to one another,<sup>21</sup> such that the direction of the lateral composition modulation becomes a preferred symmetry axis. As a result, this reduced symmetry will be reflected in the electronic band structure. For example, the interband electronic transitions in the SPS structure are expected to show preferred polarization along the modulation axis due to valence-band-splitting, and band edge electron-hole recombination is expected to occur at lower energies than the

disordered InAlAs<sub>2</sub> alloy. To study these effects, low temperature PPL measurements were performed.

Figure 6 shows the low-temperature PPL spectra taken at 10K, using the 514.5 nm line of an Ar ion laser with a power of 3 mW. The PPL emission was analyzed with a polarizer parallel to either [110] or  $[\bar{1}\bar{1}0]$ , and another polarizer parallel to [100] was placed just in front of the spectrometer to eliminate the effect of the polarization-dependent throughput of the spectrometer. The luminescence signal was dispersed by a 0.27 m single grating spectrometer and detected with a CCD detector array. The strong peak at 1.32 eV comes from the SPS layer, the peak at 1.54 eV originates from the alloy buffer layer, and the 1.47 eV peak is attributed to defects in the buffer layer. The assignment of these peaks was accomplished by selectively removing each component of the structure and examining the PPL spectra for each case. The PPL emission from the SPS is thus red-shifted by 220 meV with respect to the emission from the buffer and is strongly polarized (polarization ratio ~20) as expected for a sample exhibiting composition modulation.

The photoluminescence from the buffer is also polarized with a ratio of ~10. The high polarization in this case is not likely due to composition modulation, since none was demonstrated by either TEM or x-ray diffraction reciprocal space mapping. Biaxial strain due to a slight lattice mismatch would not cause any in-plane anisotropy. Polarized PL has been reported in zinc-blende binary compounds, however, the polarization ratio is quite small.<sup>22</sup> Instead, it is proposed that the polarization arises due to very slight double-variant CuPt ordering.<sup>23</sup> Electron diffraction patterns from the buffer show two very weak pairs of (111) diffraction spots associated with CuPt ordering along the two  $[111]_B$  directions. In single variant CuPt alloys, the anisotropy of the PPL is always less than three, but in double variant CuPt ordering this value has been predicted<sup>24</sup> to be much larger than three.

## CONCLUSIONS

Cross-sectional TEM images and x-ray diffraction space mapping have shown that the SPSs of AlAs/InAs have spontaneously formed lateral composition modulation. High magnification cross-sectional TEM indicated that the growth surface has become corrugated. Careful analysis of the image contrast revealed that the tops of the surface corrugation are Al-rich while the troughs are In-rich for lattice matched to tensile structures. X-ray diffraction and TEM showed that the films are compositionally modulated in both the  $\langle 110 \rangle$  directions, with the modulation wavelength on the order of 180Å in the [110] direction and 330Å in the  $[\bar{1}\bar{1}0]$  direction. This anisotropy most likely arises due to the reversal of the symmetry axis

of the reconstruction for the InAs and AlAs surfaces during SPS growth. PPL results show a red shift of the band-edge transitions in the compositionally modulated film, and the signal is strongly polarized in the  $[\bar{1}\bar{1}0]$  direction with an anisotropy ratio of nearly 20. The PPL emission from the buffer also exhibited an anisotropy which is attributed to very weak CuPt ordering.

## ACKNOWLEDGMENT

The authors wish to thank M.P. Moran for valuable TEM sample preparation and gratefully acknowledge the support of the U.S. Department of Energy, OER/BES Division of Materials Science Grant No. DE-AC02-83-CH10093.

## REFERENCES

1. See for example, A.G. Cullis, *MRS Bulletin* 21 (1996).
2. R.J. Asaro and W.A. Tiller, *Met. Trans.* 3, 1789 (1972).
3. D.J. Srolovitz, *Acta Metall.* 37, 621 (1989).
4. J.E. Guyer and P.W. Voorhees, *Phys. Rev. Lett.* 74, 4031 (1995).
5. J. Tersoff and F.K. LeGoues, *Phys. Rev. Lett.* 72, 3570 (1994).
6. C. Roland, *MRS Bulletin* 27 (April 1996).
7. D.E. Jesson, K.M. Chen and S.J. Pennycook, *MRS Bulletin* 31 (April 1996).
8. J. Mirecki Millunchick, R.D. Twesten, D.M. Follstaedt, S.R. Lee, E.D. Jones, Y. Zhang, H.M. Cheong, S.P. Ahrenkiel and A. Mascarenhas, *Appl. Phys. Lett.* 70, 1402 (1997).
9. J. E. Guyer and P.W. Voorhees, *Phys. Rev. B* 54, 11710 (1996).
10. A. Zunger and S. Mahajan, *Handbook on Semiconductors* 3, 1399 (Elsevier Science, 1994).
11. A. C. Chen, A.M. Moy, L.J. Chou, K.C. Hsieh and K.Y. Cheng, *Appl. Phys. Lett.* 66, 2694 (1995).
12. S. T. Chou, K.Y. Cheng, L.J. Chou and K.C. Hsieh, *J. Appl. Phys.* 78, 6270 (1995).
13. S.T. Chou, K.C. Hsieh, K.Y. Cheng and L.J. Chou, *J. Vac. Sci. Technol B* 13, 650 (1995).
14. J. Yoshida, K. Kishino, D.H. Jang, S. Nahm, I. Nomura and A. Kikochi, *Optical and Quantum Electron.* 28, 547 (1996).
15. S.R. Lee, B.L. Doyle, T.J. Drummond, J.W. Medernach and R.P. Schneider Jr., *Advances in X-Ray Analysis*, ed. P. Predecki (New York: Plenum Press, 1995), p. 201.
16. T. Hashizume, Q.K. Xue, J. Zhou, A. Ichimiya and T. Sakurai, *Phys. Rev. Lett.* 73, 2208 (1994).
17. K. Shiraishi, *Appl. Phys. Lett.* 60, 1363 (1992).
18. J.-I. Chyi, J.-L. Shieh, R.-M. Lin, T.-E. Nee and J.-W. Pan, *Appl. Phys. Lett.* 65, 699 (1994).
19. M.M.J. Treacy, J.M. Gibson and A. Howie, *Phil. Mag.* A 51, 389 (1985).
20. R.D. Twesten, J. Mirecki Millunchick, S.R. Lee, D.M. Follstaedt, E.D. Jones, S.P. Ahrenkiel, Yong Zhang, and A. Mascarenhas, *Thin Films-Structure and Morphology*, ed. S. Moss, D. Ila, R.C. Cammarata, E.H. Chason, T.L. Einstein and E.D. Williams, 441, (Pittsburgh, PA: Mater. Res. Soc., 1997), p. 187.
21. A. Mascarenhas, R.G. Alonso, G.S. Homer, S. Froyen, K.C. Hsieh and K.Y. Cheng, *Phys. Rev. B* 48, 4907 (1993).
22. K.Y. Cheng, K.C. Hsieh, J.N. Baillargeon and A. Mascarenhas, *Inst. Phys. Conf. Ser.*, 120 (Bristol: Inst. of Phys., 1991), p. 589.
23. A. Mascarenhas, Y. Zhang, R.G. Alonso and S. Froyen, *Solid State Comm.* 100, 47 (1997).
24. Y. Zhang and A. Mascarenhas, unpublished.